Heliyon 9 (2023) e21401

Contents lists available at ScienceDirect

Heliyon

journal homepage: www.cell.com/heliyon

Research article

A paradigmatic approach to the molecular descriptor computation for some antiviral drugs

Muhammad Usman Ghani [a], Muhammad Imran [b,*], S. Sampathkumar [c], Fairouz Tchier [d], K. Pattabiraman [e], Ahmad Zubair Jan [f]

[a] Institute of Mathematics, Khawaja Fareed University of Engineering & Information Technology, Abu Dhabi Road, 64200, Rahim Yar Khan, Pakistan
[b] Department of Mathematical Sciences, United Arab Emirates University, Al Ain, United Arab Emirates
[c] Department of Mathematics, SSN College of Engineering, Kalvakkam - 603 110, India
[d] Mathematics Department, College of Science, King Saud University, P.O. Box 22452, Riyadh 11495, Saudi Arabia
[e] Department of Mathematics Government Arts College, Kumbakonam 612 002, India
[f] Wroclaw University of Science and Technology, Faculty of Mechanical Engineering, Poland

ARTICLE INFO

Keywords:
Irregularity indices
Antiviral drugs
Edge partition
Topological indices
Graph polynomials

ABSTRACT

In theoretical chemistry, topological indices are commonly employed to model the physico-chemical properties of chemical compounds. Mathematicians frequently use Zagreb indices to calculate a chemical compound's strain energy, melting point, boiling temperature, distortion, and stability. The current global pandemic caused by the new SARS-CoV-2, also known as COVID-19, is a significant public health concern. Various therapy modalities are advised. The issue has become worse since there hasn't been enough counseling. Researchers are looking at compounds that might be used as SARS and MERS therapies based on earlier studies. In several quantitative structure-property-activity relationships (QSPR and QSAR) studies, a variety of physiochemical properties are successfully represented by topological indices, a sort of molecular descriptor that just specifies numerical values connected to a substance's molecular structure. This study investigates several irregularity-based topological indices for various antiviral medicines, depending on the degree of irregularity. In order to evaluate the effectiveness of the generated topological indices, a QSPR was also carried out using the indicated pharmaceuticals, the various topological indices, and the various physiochemical features of these antiviral medicines. The acquired results show a substantial association between the topological indices being studied by the curve-fitting approach and the physiochemical properties of possible antiviral medicines.

1. Introduction

The SARS-CoV-2 virus strain is the source of the infectious disease coronavirus disease 2019 (COVID-19), which is also known as COVID-19 [1]. In 2019, in Wuhan, China, the first COVID-19 case was reported. Since then, instances have spread internationally, causing the coronavirus pandemic crisis between 2019 and 2020 [2]. In the spectrum of identified cases, there will be four deaths

* Corresponding author.
E-mail address: imrandhab@gmail.com (M. Imran).

https://doi.org/10.1016/j.heliyon.2023.e21401
Received 20 July 2023; Received in revised form 5 October 2023; Accepted 20 October 2023

Available online 27 October 2023

List of Abbreviations

QSPR	quantitative structure–property relationships	$\mu_G(x)$	Degree vertices of x
QSAR	quantitative structure–activity relationships	$\mu_G(x)$	Degree vertices of y
PHEIC	Public Health Emergency of International Concern	BP	Boiling Point
WHO	World Health Organization	MV	Molar volume
CT(Scan)	Computed Tomography Scan	FP	Flash point
GLOPID-R	Global Research Collaborative on Infectious Disease Preparedness	T	Surface Tension
M_1	First Zagreb	PSA	Polar Surface Area
M_2	Second Zagreb	P	Polarizability

up until March 2020, according to [3]. The 2019–2020 coronavirus outbreak has been declared a pandemic and a Public Health Emergency of International Concern (PHEIC) by the World Health Organisation (WHO) [4]. In many countries throughout each of the six WHO regions, there is proof of close disease transmission. Infected people frequently have symptoms including fever, coughing, and shortness of breath; however, less often seen symptoms include muscular discomfort, sputum production, and raw throat. While most instances have mild symptoms, some develop severe pneumonia and multi-organ failure [5]. According to [6], the virus frequently spreads from one person to another by respiratory droplets made while coughing and sneezing. Typically, it takes 2 to 14 days from exposure to the start of symptoms, with a mean of 5 days [7]. A chest computed tomography scan (CT scan) that shows potential respiratory diseases can be used to detect the infection in addition to a combination of symptoms, risk factors, and these tests. For persons who are suspected of having the virus and their caretakers, but not for the general public, suggested infection prevention methods include regular hand washing, social withdrawal, keeping hands away from the face, and mask-wearing [8]. Coronavirus is not currently being treated with a vaccine or any specialized antiviral medications. However, management includes symptom therapy, follow-up care, seclusion, and experimental methods.

Comparing existing experimental data on topological indices can be a complex task, as it depends on the specific indices being considered, the types of molecules or structures they are applied to, and the sources of data available. Topological indices are mathematical descriptors that provide information about the structure of molecules or networks, and they can have various applications in chemistry, biology, and materials science. Some common topological indices include the Wiener index, the Randic index, and the Zagreb indices, among others. For this, we observed select molecules or structures, collected experimental data, calculated topological indices, performed statistical analysis, etc. The COVID-19 pandemic poses a serious threat to the global public health infrastructure. The whole community became more aware of the worst-case possibilities as the number of instances, patients, and fatalities increased globally. In order to combat the COVID-19 pandemic, the medical and scientific communities are working together to collect the most up-to-date information available through diagnosis, treatment, and management procedures. The COVID-19 Study Roadmap was created in January 2020 by the WHO in collaboration with the Global Research Collaborative on Infectious Disease Preparedness (GLOPID-R) (www.glopid-r.org). There is no established plan for treating COVID-19 individuals, despite awareness of the SARS-CoV-2 infectious cycle. In the meantime, researchers from all around the world are working hard to develop therapeutic medicines or vaccines against viruses. Numerous novel medications that have shown antiviral activity against SARS-CoV-2 were studied in the study based on current scientific findings and recommendations. Every year, chemical laboratories produce a sizeable fraction of new pharmaceuticals and medicines that are then released into the market following research trials. In order to determine their toxicity, side effects, and biological activity on the human body, several tests and studies are first required. For nations with limited resources, testing these medications would be exceedingly expensive and would require expensive laboratories. Researchers studied a sizable number of chemical compounds and examined their molecular structures to draw conclusions about the qualities of drugs. Numerous scientific research studies have shown a substantial correlation between the qualities of medications or treatments and their molecular structure. Drugs' medicinal qualities can be derived by applying chemical graph theory [19,21,44] to the molecular structure of the relevant medication. Chemical graph theory is a branch of mathematical chemistry that integrates math, chemistry, and graph theory to quantitatively resolve chemistry-related problems [9–11]. A topological index is a type of molecular descriptor that is commonly used in quantitative structure-property/activity relationship (QSPR/QSAR) studies. It is an efficient way to model many physicochemical properties by simply defining numerical values associated with the molecular structure of a compound [25,12,27,13]. The further study on this subject were presented in [29,14,15,34]. Further discussed in this paper is an analysis of the topological indices provided above using QSPR. We demonstrate, using the polynomial regression approach, that the obtained attributes are significantly related to the properties of COVID-19 antiviral medications.

Applications of molecular descriptors in chemistry:

Molecular descriptors, also known as molecular indices or molecular features, are numerical representations that capture various properties and characteristics of molecules [30,31]. These descriptors play a significant role in a wide range of applications in chemistry, bioinformatics, drug discovery, materials science, and other fields. Here are some common applications of molecular descriptors:

(i) Quantitative Structure-Activity Relationship (QSAR) Studies: Molecular descriptors are used in QSAR studies to establish relationships between the chemical structure of a molecule and its biological activity. This is valuable in drug design, predicting biological effects, and understanding molecular interactions.
(ii) Drug Design and Discovery: Molecular descriptors help in designing new drug candidates by predicting their properties, such as solubility, bioavailability, toxicity, and binding affinity to target proteins. These predictions aid in selecting promising candidates for further development.
(iii) Virtual Screening: Molecular descriptors are employed in virtual screening processes to prioritize compounds from large chemical libraries. Descriptors can be used to filter out molecules that are less likely to be successful drug candidates.
(iv) Quantitative Structure-Property Relationship (QSPR) Studies: Similar to QSAR, QSPR involves using molecular descriptors to establish relationships between molecular structure and physical or chemical properties, such as boiling point, melting point, refractive index, and more.
(v) Material Design and Discovery: Molecular descriptors are used in materials science to predict properties of materials, such as electronic properties, conductance, and thermal stability. This aids in designing new materials with specific desired properties.
(vi) Environmental Chemistry: Molecular descriptors can be used to predict the environmental behavior of molecules, such as their persistence, bioaccumulation, and potential toxicity.
(vii) Cheminformatics and Bioinformatics: In cheminformatics and bioinformatics, molecular descriptors are used for data analysis, similarity searching, clustering, and classification of compounds.
(viii) Toxicity Prediction: Molecular descriptors contribute to toxicity prediction models, helping to identify potential hazardous compounds and prioritize safety assessments.
(ix) Quantum Chemistry and Computational Chemistry: Molecular descriptors are sometimes used as input features for quantum chemical calculations and molecular modeling, aiding in simulating molecular properties and behavior.
(x) Analytical Chemistry: Molecular descriptors can be used to develop calibration models for analytical techniques like spectroscopy and chromatography.
(xi) Molecular Visualization and Communication: Descriptors can be used to visualize and communicate molecular properties in a simplified form to researchers, making complex molecular information more accessible.
(xii) Machine Learning and Data Mining: Molecular descriptors serve as input features for machine learning algorithms, facilitating the development of predictive models and pattern recognition.

These are just a few examples of the diverse applications of molecular descriptors. Their versatility and ability to capture essential molecular information make them fundamental tools in various scientific and industrial domains.

2. Graph-theoretical preliminaries

The graph theory concepts that must be understood in order to establish the conclusions in the next parts are listed in this section, [38,39]. These definitions might be used to create reliable machine learning and artificial intelligence techniques for a vast combinatorial library of medications. A molecular graph is a straightforward graph in which the vertices and edges represent, respectively, the atoms and bonds of the substance. Allow G to stand for a graph with a set of vertices $V(G)$ whose cardinality is α and subsets of two elements called the edges constituting $E(G)$, whose cardinality equals the size β, of $V(G)$. In 1975, Gutman provided the concept of Zagreb indices, and they have given the definition of the first and second Zagreb indices, which are defined as

$M_1(G) = \sum_{xy \in E(G)} (\mu_G(x) + \mu_G(y))$ and $M_2(G) = \sum_{xy \in E(G)} \mu_G(x)\mu_G(y)$, where $\mu_G(x)$ and $\mu_G(y)$ are degrees of vertices x and y in G, respectively.

If specific criteria are satisfied, topological indices are regarded as irregularity indices. The topological indices of a graph must first be larger than or equal to zero. Second, if a graph's topological indices are equal to zero, it is assumed that the graph is regular. The irregularity indices of a connected graph G with α vertices and β edges are defined as follows;

1. $VAR(G) = \sum_{x \in V(G)} \left(\mu_G(x) - \frac{2\beta}{\alpha}\right)^2$
2. $AL(G) = \sum_{xy \in E(G)} \left|\mu_G(x) - \mu_G(y)\right|$
3. $IR_1(G) = \sum_{x \in V(G)} \mu_G(x)^3 - \left(\frac{2\beta}{\alpha}\right) \sum_{x \in V(G)} \mu_G(x)^2$
4. $IR_2(G) = \sqrt{\sum_{xy \in E(G)} \frac{\mu_G(x)\mu_G(y)}{\beta} - \frac{2\beta}{\alpha}}$
5. $IRF(G) = \sum_{xy \in E(G)} (\mu_G(x) - \mu_G(y))^2$
6. $IRFW(G) = \frac{IRF(G)}{M_2(G)}$
7. $IRA(G) = \sum_{xy \in E(G)} (\mu_G(x)^{-\frac{1}{2}} - \mu_G(y)^{-\frac{1}{2}})^2$
8. $IRB(G) = \sum_{xy \in E(G)} (\mu_G(x)^{\frac{1}{2}} - \mu_G(y)^{\frac{1}{2}})^2$

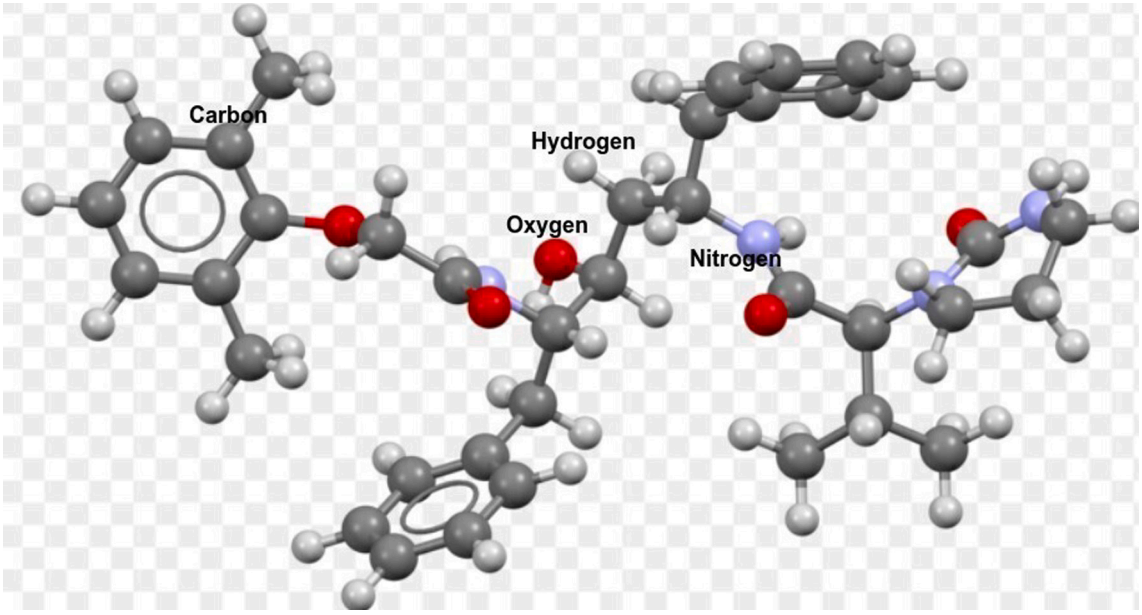

Fig. 1. Molecular structure of Lopinavir/Ritonavir ($C_{37}H_{48}N_4O_5$)

9. $IRC(G) = \sum_{xy \in E(G)} \frac{\sqrt{\mu_G(x)\mu_G(y)}}{m} - \frac{2\beta}{\alpha}$
10. $IRDIF(G) = \sum_{xy \in E(G)} \left| \frac{\mu_G(x)}{\mu_G(y)} - \frac{\mu_G(y)}{\mu_G(x)} \right|$
11. $IRL(G) = \sum_{xy \in E(G)} \left| ln\,\mu_G(x) - ln\,\mu_G(y) \right|$
12. $IRLU(G) = \sum_{xy \in E(G)} \frac{|\mu_G(x) - \mu_G(y)|}{min\{\mu_G(x), \mu_G(y)\}}$
13. $IRLF(G) = \sum_{xy \in E(G)} \frac{|\mu_G(x) - \mu_G(y)|}{\sqrt{\mu_G(x)\mu_G(y)}}$
14. $IRLA(G) = 2 \sum_{xy \in E(G)} \frac{|\mu_G(x) - \mu_G(y)|}{\mu_G(x) + \mu_G(y)}$
15. $IRD_1(G) = \sum_{xy \in E(G)} ln\{1 + \left|\mu_G(x) - \mu_G(y)\right|\}$
16. $IRGA(G) = \sum_{xy \in E(G)} ln\{ \frac{\mu_G(x) + \mu_G(y)}{2\sqrt{\mu_G(x)\mu_G(y)}} \}$

3. Methodology and main results

The formulae for the relevant irregularity indices of the molecular graphs of the eight antiviral medications used in the treatment of COVID-19 are derived in this section using combinatorial computing, edge partitioning, and degree counting. First, we establish the sixteen irregularity indices of the Lopinavir molecular graph.

3.1. Clinically used drugs

Being a virus that spreads quickly, SARS-CoV-2, it is essential to treat people who are affected as soon as possible. Here is a list of some of the most popular medicines.

1. **Lopinavir/Ritonavir**
   Lopinavir (see Fig. 1) is a protease inhibitor that specifically targets the HIV virus. The FDA approved it in 2000 after it was found in 1998. This drug inhibits proteolytic processing and blocks the generation of viral proteins by imitating the structure of a peptide that HIV protease has cut. This medication, when used with oseltamivir, another flu medication, was found to result in full recovery after exhibiting pneumonia-related COVID-19 symptoms [16,17].
2. **Remidesivir (anti-viral peptide)**
   This drug (see Fig. 2), SARS-CoV, MERS-CoV, and Ebola have all been treated with an adenosine nucleotide association... In a recent study, Remidesivir scored 0.77M at half maximum dose against COVID-19 and halted the spread of viruses [18].

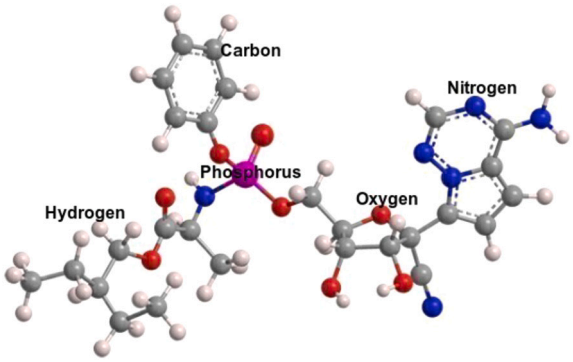

Fig. 2. Molecular structure of Remidesivir ($C_{27}H_{35}N_6O_8P$)

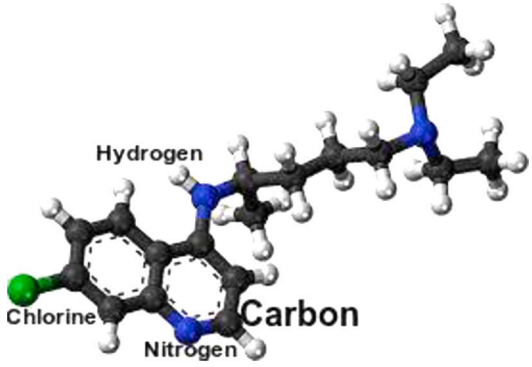

Fig. 3. Molecular structure of Chloroquine ($C_{18}H_{26}ClN_3$)

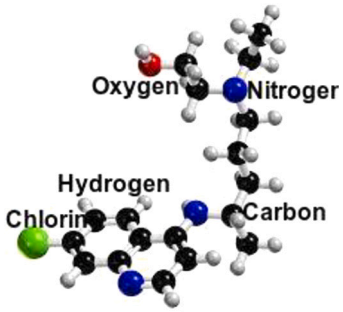

Fig. 4. Molecular structure of Hydroxychloroquine ($C_{18}H_{26}ClN_3O$)

3. **Chloroquine**
   This anti-malarial medication has demonstrated potential as a method of treating influenza A vulvaris (Yan et al., 2013). The immune system is modulated by the antiviral medication chloroquine (see Fig. 3). By increasing the endosomal PH required for viral fusion, this drug prevented viral infection and showed 1.13M against SARS-CoV-2 at half the recommended dose [20].
4. **Hydroxychloroquine**
   Its antiviral properties are extremely comparable to those of chloroquine. (see Fig. 4). Both have immune-modifying qualities that may improve their in vivo antiviral effects. According to a Forbes article dated March 30, 2020, the FDA has approved hydroxylchloroquine as an urgent coronavirus therapy. By preventing T cell activation, hydroxychloroquine reduces the cytokine storm and decreases the initial course of COVID-19 [22].
5. **Theaflavin**
   It is a molecule of polyphenol (see Fig. 5) found in that has been connected to the advantages associated with consuming black tea and has demonstrated antiviral activity against several viruses, including influenza A, B, and C [23,24].
6. **Arbidol**
   With signs of effectiveness against severe acute respiratory syndrome in vitro, arbidol, a conventional antiviral drug, is becoming more popular as a COVID-19 therapy, see Fig. 6.

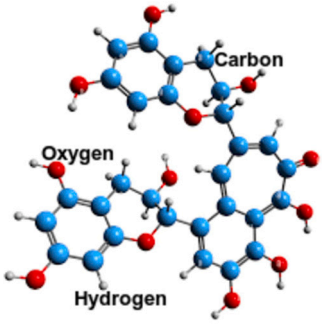

Fig. 5. Molecular structure of Theaflavin ($C_{29}H_{24}O_{12}$)

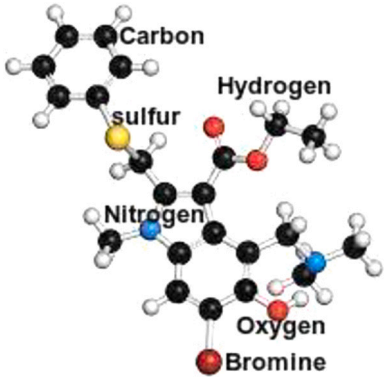

Fig. 6. Molecular structure of Arbidol($C_{22}H_{25}BrN_2O_3S$)

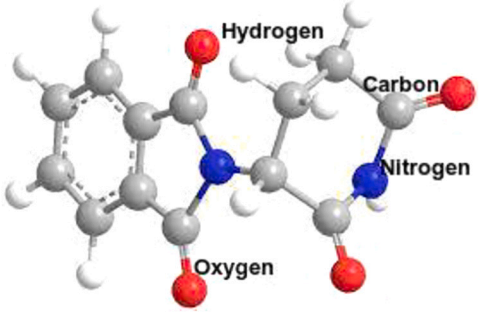

Fig. 7. Molecular structure of Arbidol($C_{13}H_{10}N_2O_4$)

Table 1
Partition of edge set of molecular graph of Lopinavir.

Edge Partition $(\mu_L(x), \mu_L(y))$	(1,3)	(2,2)	(2,3)	(3,3)
Frequency	8	14	20	7

7. Thalidomide

A potential drug for the treatment of COVID-19 patients with severe symptoms is thalidomide (see Fig. 7). The patient's oxygen index was rapidly improved, and combining 100 mg of thalidomide with a little dose of methylprednisolone allowed for the management of the development of any adverse effects. [26,28,32].

Result and Method.

Let L be a molecular graph of Lopinavir (see Fig. 8 and Fig. 9) with $\alpha = 46$ vertices and $\beta = 49$ edges. By the structure analysis of L, we have the following Table 1.

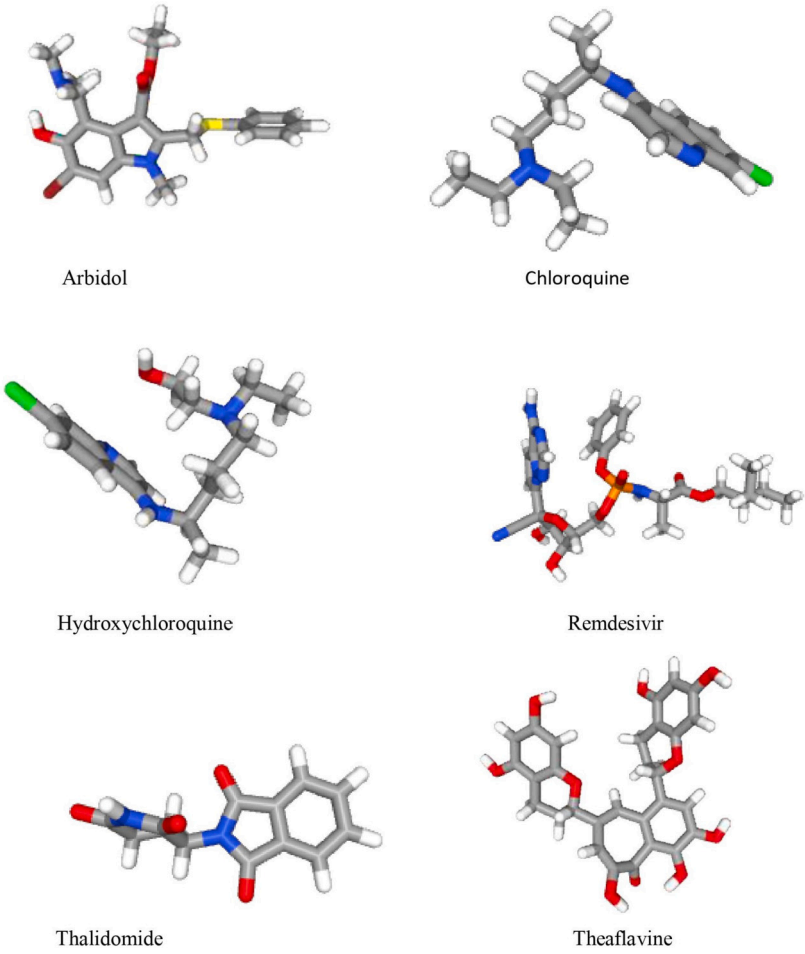

Fig. 8. The chemical structures of COVID-19 drugs

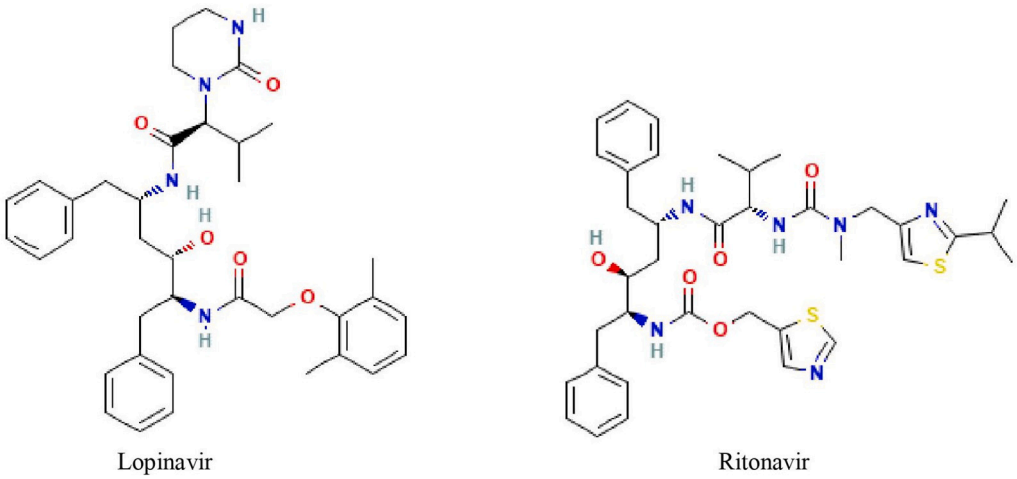

Fig. 9. The chemical structures of Lopinavir and Ritonavir

By the definitions of irregularity indices, we obtain;

$$VAR(L) = \sum_{x \in V(L)} \left(\mu_L(x) - \frac{2\beta}{\alpha}\right)^2 = \frac{M_1(L)}{\alpha} - \left(\frac{2\beta}{\alpha}\right)^2 = \frac{230}{46} - \left(\frac{2\times 49}{46}\right)^2 = 0.4614.$$

$$AL(L) = \sum_{xy\in E(L)} \left|\mu_L(x) - \mu_L(y)\right|$$
$$= 8\times|1-3| + 14\times|2-2| + 20\times|2-3| + 7\times|3-3|$$
$$= 36.$$

$$IR_1(L) = \sum_{x\in V(L)} \mu_L(x)^3 - \left(\frac{2\beta}{\alpha}\right)\sum_{x\in V(L)} \mu_L(x)^2$$
$$= F(L) - \left(\frac{2\beta}{\alpha}\right)M_1(L)$$
$$= 578 - \left(\frac{2\times 49}{46}\right)\times 230 = 88.$$

$$IR_2(L) = \sqrt{\sum_{xy\in E(L)} \frac{\mu_L(x)\mu_L(y)}{\beta}} - \left(\frac{2\beta}{\alpha}\right)$$
$$= \sqrt{\frac{M_2(L)}{\beta}} - \left(\frac{2\beta}{\alpha}\right)$$
$$= \sqrt{\frac{255}{49}} - \left(\frac{2\times 49}{46}\right) = 0.1508.$$

$$IRF(L) = \sum_{xy\in E(L)} (\mu_L(x) - \mu_L(y))^2$$
$$= \sum_{xy\in E(L)} (\mu_L(x)^2 + \mu_L(y)^2 - 2\mu_G(x)\mu_L(y))$$
$$= \sum_{xy\in E(L)} (\mu_L(x)^2 + \mu_L(y)^2) - 2\sum_{xy\in E(L)} \mu_L(x)\mu_L(y)$$
$$= F(L) - 2M_2(L) = 578 - 2\times 255 = 68.$$

$$IRFW(L) = \frac{IRF(L)}{M_2(L)} = \frac{68}{255} = 0.2666.$$

$$IRA(L) = \sum_{xy\in E(L)} \left(\mu_L(x)^{-\frac{1}{2}} - \mu_L(y)^{-\frac{1}{2}}\right)^2$$
$$= \sum_{xy\in E(L)} \left(\frac{1}{\mu_L(x)} + \frac{1}{\mu_L(y)} - \frac{2}{\sqrt{\mu_L(x)\mu_L(y)}}\right)$$
$$= \sum_{xy\in E(L)} \left(\frac{1}{\mu_L(x)} + \frac{1}{\mu_L(y)}\right) - \sum_{xy\in E(L)} \frac{2}{\sqrt{\mu_L(x)\mu_L(y)}}$$
$$= \alpha - 2\left(8\times\frac{1}{\sqrt{1\times 3}} + 14\times\frac{1}{\sqrt{2\times 2}} + 20\times\frac{1}{\sqrt{2\times 3}} + 7\times\frac{1}{\sqrt{3\times 3}}\right)$$
$$= 46 - 44.2342 = 1.7658.$$

$$IRB(L) = \sum_{xy\in E(L)} \left(\mu_L(x)^{\frac{1}{2}} - \mu_L(y)^{\frac{1}{2}}\right)^2$$
$$= \sum_{xy\in E(L)} \left(\mu_L(x) + \mu_L(y)) - 2\sqrt{\mu_L(x)\mu_L(y)}\right)$$
$$= M_1(L) - 2\sum_{xy\in E(L)} \sqrt{\mu_L(x)\mu_L(y)}$$
$$= M_1(L) - 2\left(8\times\sqrt{1\times 3} + 14\times\sqrt{2\times 2} + 20\times\sqrt{2\times 3} + 7\times\sqrt{3\times 3}\right)$$
$$= 230 - 2\times 111.846 = 6.308.$$

$$IRC(L) = \sum_{xy\in E(L)} \frac{\sqrt{\mu_L(x)\mu_L(y)}}{\beta} - \left(\frac{2\beta}{\alpha}\right) = \frac{111.846}{49} - \frac{2\times 49}{46} = 0.1522.$$

$$IRDIF(L) = \sum_{xy\in E(L)} \left|\frac{\mu_L(x)}{\mu_L(y)} - \frac{\mu_L(y)}{\mu_L(x)}\right|$$
$$= 8\times\left|\frac{1}{3} - \frac{3}{1}\right| + 14\times\left|\frac{2}{2} - \frac{2}{2}\right| + 20\times\left|\frac{2}{3} - \frac{3}{2}\right| + 7\times\left|\frac{3}{3} - \frac{3}{3}\right|$$
$$= 3.7999.$$

Table 2
Partition of edge set of molecular graph of Ritonavir.

Edge Partition $(\mu_G(x), \mu_G(y))$	(1,3)	(2,2)	(2,3)	(3,3)
Frequency	9	13	26	5

$$IRL(L) = \sum_{xy\in E(L)} |ln\,\mu_L(x) - ln\,\mu_L(y)|$$
$$= 8\times|ln\,1 - ln\,3| + 14\times|ln\,2 - ln\,2| + 20\times|ln\,2 - ln\,3| + 7\times|ln\,3 - ln\,3|$$
$$= 8\times(0 - 1.0986) + 20\times(0.6931 - 1.0986) = 16.8988.$$

$$IRLU(L) = \sum_{xy\in E(L)} \frac{|\mu_L(x) - \mu_L(y)|}{min\{\mu_L(x), \mu_L(y)\}} = 8\times\frac{2}{1} + 14\times\frac{0}{2} + 20\times\frac{1}{2} + 7\times\frac{0}{3} = 26.$$

$$IRLF(L) = \sum_{xy\in E(L)} \frac{|\mu_L(x) - \mu_L(y)|}{\sqrt{\mu_L(x)\mu_L(y)}} = 8\times\frac{2}{\sqrt{3}} + 14\times\frac{0}{\sqrt{4}} + 20\times\frac{1}{\sqrt{6}} + 7\times\frac{0}{\sqrt{9}} = 17.4028.$$

$$IRLA(L) = 2\sum_{xy\in E(L)} \frac{|\mu_L(x) - \mu_L(y)|}{\mu_L(x) + \mu_L(y)} = 2\left(8\times\frac{2}{4} + 14\times\frac{0}{4} + 20\times\frac{1}{5} + 7\times\frac{0}{6}\right) = 16.$$

$$IRD_1(L) = \sum_{xy\in E(L)} ln\{1 + |\mu_L(x) - \mu_L(y)|\}$$
$$= 8\times ln\{1+2\} + 14\times ln\{1+0\} + 20\times ln\{1+1\} + 7\times ln\{1+0\}$$
$$= 8\times 1.0986 + 14\times 0 + 20\times 0.6931 + 7\times 0$$
$$= 8.7888 + 13.862 = 22.6508.$$

$$IRGA(L) = \sum_{xy\in E(L)} ln\{\frac{\mu_L(x) + \mu_L(y)}{2\sqrt{\mu_L(x)\mu_L(y)}}\}$$
$$= 8\times ln\{\frac{2}{3}\} + 14\times ln\{1\} + 20\times ln\{\frac{5}{2\sqrt{6}}\} + 7\times ln\{1\}$$
$$= 1.5584.$$

Next we obtain the irregularity indices of Ritonavir.

Let G be a Ritonavir's molecular graph (see Fig. 1) with 50 vertices and 53 edges, that is, $alpha = 50$ and $beta = 53$ as determined by its structure [33,35,36]. By the structure analysis of G, we have the following Table 2.

By the definitions of irregularity indices, we obtain;

$$VAR(G) = \frac{M_1(G)}{\alpha} - \left(\frac{2\beta}{\alpha}\right)^2 = \frac{248}{50} - \left(\frac{2\times 53}{50}\right)^2 = 0.4656.$$

$$AL(G) = \sum_{xy\in E(G)} |\mu_G(x) - \mu_G(y)| = 44.$$

$$IR_1(G) = F(G) - \left(\frac{2\beta}{\alpha}\right)M_1(G) = 622 - \left(\frac{2\times 53}{50}\right)\times 248 = 96.24.$$

$$IR_2(G) = \sqrt{\frac{M_2(G)}{\beta}} - \left(\frac{2\beta}{\alpha}\right) = \sqrt{\frac{255}{53}} - \left(\frac{2\times 53}{50}\right) = 0.0735.$$

$$IRF(G) = F(G) - 2M_2(G) = 622 - 2\times 255 = 112.$$

$$IRFW(G) = \frac{IRF(G)}{M_2(G)} = \frac{112}{255} = 0.4392.$$

$$IRA(G) = \sum_{xy\in E(G)} \left(\frac{1}{\mu_G(x)} + \frac{1}{\mu_G(y)}\right) - 2\sum_{xy\in E(G)} \frac{1}{\sqrt{\mu_G(x)\mu_G(y)}}$$
$$= \alpha - 2\left(9\times\frac{1}{\sqrt{1\times 3}} + 13\times\frac{1}{\sqrt{2\times 2}} + 26\times\frac{1}{\sqrt{2\times 3}} + 5\times\frac{1}{\sqrt{3\times 3}}\right)$$
$$= 2.0454.$$

$$IRB(G) = M_1(G) - 2\sqrt{\mu_G(x)\mu_G(y)} = 248 - 2\times 62.9567 = 122.0866.$$

$$IRC(G) = \frac{62.9567}{53} - \left(\frac{2\times 53}{50}\right) = 0.9322.$$

$$IRDIF(G) = 9\times\left|\frac{1}{3} - \frac{3}{1}\right| + 26\times\left|\frac{2}{3} - \frac{3}{2}\right| = 45.6666.$$

Table 3
Partition of edge set of some molecular graphs.

$(\mu(x), \mu(y))$	Arbidol	Thalidomide	Remsesivir	Chloroquine	H-chloroquine	Theaflavin
(1,2)	1	-	2	2	2	-
(1,3)	6	4	5	2	2	10
(1,4)	-	-	2	-	-	-
(2,2)	6	4	9	5	6	-
(2,3)	9	6	14	12	12	22
(2,4)	-	-	4	-	-	-
(3,3)	9	7	6	2	2	14
(3,4)	-	-	2	-	-	-
Total Frequency	31	21	44	23	24	46

Table 4
Topological descriptors and their values of molecular graphs of the drugs.

TDs	Lopinavir	Ritonavir	Arbidol	Thalidomide	Chloroquine	H-Chloroquine	Theaflavin	Remdesivir
VAR	0.4614	0.4656	0.6018	0.5874	0.6617	0.4464	0.4275	0.6722
AL	36	44	22	14	42	18	18	42
IR_1	88	96.24	71.315	46.108	122.3992	40.3646	40.441	112.9274
IR_2	0.1508	0.0735	0.265	0.2487	0.2705	0.1932	0.1861	0.2583
IRF	68	112	34	22	72	22	22	62
IRFW	0.2666	0.4392	0.1899	0.1732	0.2801	0.1833	0.1774	0.2153
IRA	1.7658	2.0454	7.0826	0.8154	1.984	7.0644	0.7312	0.2153
IRB	6.308	122.0866	4.2966	2.75	7.954	34.6272	2.6272	2.1566
IRC	0.1522	0.9322	0.2121	0.2002	0.2178	0.5397	0.15	0.2172
IRDIF	3.7999	45.6666	57	15.6666	42.6666	18.3333	18.3333	20.9999
IRL	16.8988	20.4304	10.9342	6.8274	18.677	8.4494	8.4494	19.907
IRLU	26	31	17.5	11	29.6666	12	12	31
IRLF	17.4028	21.007	11.3097	7.0684	19.3091	8.6226	8.6226	20.5287
IRLA	16	94.09	5.4666	6.4	20.238	7.1332	7.1332	18.8
IRD_1	22.6508	27.908	7.5226	8.553	16.8186	11.9006	11.9006	26.2342
IRGA	1.5584	1.8246	1.1053	0.6976	1.8248	06502	06502	1.8868

$$IRL(G) = \sum_{xy\in E(G)} \left|ln\,\mu_G(x) - ln\,\mu_G(y)\right|$$
$$= 9\times|ln\,1 - ln\,3| + 26\times|ln\,2 - ln\,3|$$
$$= 9\times(0 - 1.0986) + 26\times(0.6931 - 1.0986) = 20.4304.$$

$$IRLU(G) = \sum_{xy\in E(G)} \frac{\left|\mu_G(x) - \mu_G(y)\right|}{min\{\mu_G(x), \mu_G(y)\}} = 9\times\frac{2}{1} + 26\times\frac{1}{2} = 31.$$

$$IRLF(G) = \sum_{xy\in E(G)} \frac{\left|\mu_G(x) - \mu_G(y)\right|}{\sqrt{\mu_G(x)\mu_G(y)}} = 9\times\frac{2}{\sqrt{3}} + 26\times\frac{1}{\sqrt{6}} = 21.007.$$

$$IRLA(G) = 2\sum_{xy\in E(G)} \frac{\left|\mu_G(x) - \mu_G(y)\right|}{\mu_G(x) + \mu_G(y)} = 2\left(9\times\frac{2}{4} + 26\times\frac{1}{5}\right) = 94.09.$$

$$IRD_1(G) = \sum_{xy\in E(G)} ln\{1 + \left|\mu_G(x) - \mu_G(y)\right|\}$$
$$= 9\times ln\{3\} + 13\times ln\{1\} + 26\times ln\{2\} + 5\times ln\{1\}$$
$$= 27.908.$$

$$IRGA(G) = \sum_{xy\in E(G)} ln\{\frac{\mu_G(x) + \mu_G(y)}{2\sqrt{\mu_G(x)\mu_G(y)}}\}$$
$$= 9\times ln\{\frac{2}{\sqrt{3}}\} + 13\times ln\{1\} + 26\times ln\{\frac{5}{2\sqrt{6}}\} + 5\times ln\{1\}$$
$$= 1.8246.$$

Table 3 shows that the edge partitions of vertex degrees for the molecular graphs of the proposed drugs given in Fig. 1.

For all the drugs considered we now list the irregularity indices are derived as in the case of Lopinavir and Ritonavir. These are listed below in the follow table.

Table 5
Physico-chemical properties of COVID-19 drugs.

Drugs	BP	E	FP	MR	PSA	P	T	MV
Lopinavir	924.2	1408	5127	1792	120	710	495	5405
Ritonavir	9470	1444	5266	1989	202	789	537	5817
Arbidol	5918	915	3117	1219	80	483	453	3473
Thalidomide	4878	794	2488	652	87	257	716	161
Chloroquine	4606	721	2323	974	28	386	440	2879
Hydroxy-Chloroquine	5167	830	2663	990	48	392	498	2854
Theaflavin	10039	1535	3365	1373	218	544	1386	3010
Remdesivir	-	-	-	1495	213	593	623	409

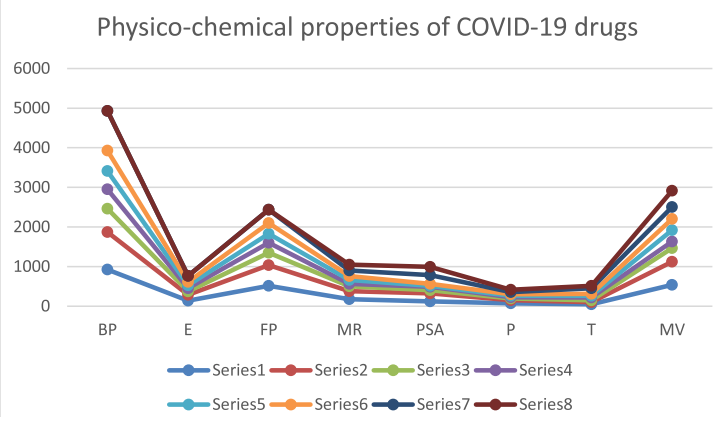

Fig. 10. Graphical representation of Physico-chemical properties of COVID-19 drugs

4. QSPR/QSAR analysis for anticovid drugs

This section's main objective is to develop a quantitative structure-property relationship (QSPR) between the various irregularity-based topological indices and particular physicochemical properties in Table 5 and graphically in Fig. 10 of the medications under investigation in order to evaluate the effectiveness of the topological indices [37,40,41]. In order to model antiviral activity using sixteen irregularity-based topological indices, eight representative physicochemical properties including boiling point (BP), enthalpy of vaporisation (E), flash point (FP), molar refraction (MR), polar surface area (PSA), polarizability (P), surface tension (T), and molar volume (MV) were used.

We list the measured values of the irregularity-based topological indices for the COVID-19 medications derived in Table 4. The physicochemical properties of the proposed drugs are listed in Table 5. For each plot, we performed polynomial fitting in order to generate an equation. Table 6 shows the adj. R^2 value for each plot. For boiling point, enthalpy, FP, MR, PSA, and P, it can be shown that the VAR descriptor has the best value (that is, adj. R^2 is closest to 1), respectively [42,43]. The highest value of adj. R^2 ensures the best fit for the data, and, as a result, the equation produced from it has the least amount of inaccuracy. For T, the VAR and IR_2 descriptors are higher predictions and have the best adj. R^2 values, which are close to 1. Finally, for the property Molar Volume (MV), the $VAR, IR_1, IRDIF, IRL, IRLF, IRLA$, and IRD_1 are the suitable predictors that have the higher adj. R^2 values close to 1. Among these, IRL is the best-suited predictor for molar volume.
The equation obtained between BP vs VAR is as follows;

$$BP = \alpha_6(VAR)^6 - \alpha_5(VAR)^5 + \alpha_4(VAR)^4 - \alpha_3(VAR)^3 + \alpha_2(VAR)^2 - \alpha_1(VAR) + \beta, \tag{1}$$

where $\alpha_6 = 1166160569.0887$, $\alpha_5 = 4044449970.9457$, $\alpha_4 = 5799985647.1694$,

$\alpha_3 = 4402008812.7206, \alpha_2 = 1864808742.3685, \alpha_1 = 418059537.0011$and $\beta = 38748951.7427$.

The equation obtained between E vs VAR is as follows;

$$E = \alpha_6(VAR)^6 - \alpha_5(VAR)^5 + \alpha_4(VAR)^4 - \alpha_3(VAR)^3 + \alpha_2(VAR)^2 - \alpha_1(VAR) + \beta_1, \tag{2}$$

where $\alpha_6 = 149113137.2664$, $\alpha_5 = 521405225.1238$, $\alpha_4 = 753314513.3290$,

$\alpha_3 = 575632846.2723, \alpha_2 = 245366473.7467, \alpha_1 = 55318493.139$ and $\beta_1 = 5153835.7661$.

The equation obtained between FP vs VAR is as follows;

$$FP = \alpha_6(VAR)^6 - \alpha_5(VAR)^5 + \alpha_4(VAR)^4 - \alpha_3(VAR)^3 + \alpha_2(VAR)^2 - \alpha_1(VAR) + \beta_2, \tag{3}$$

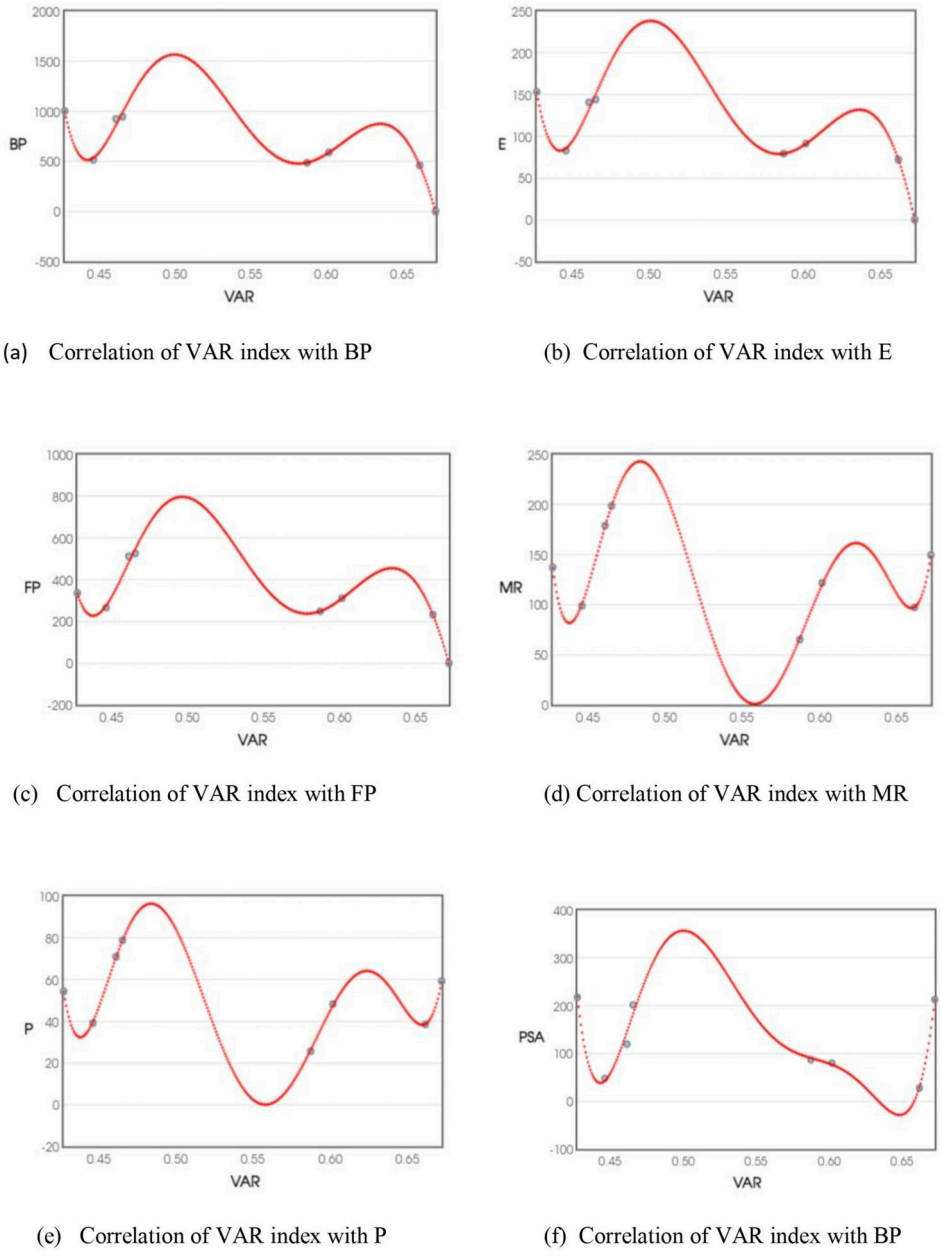

(a) Correlation of VAR index with BP

(b) Correlation of VAR index with E

(c) Correlation of VAR index with FP

(d) Correlation of VAR index with MR

(e) Correlation of VAR index with P

(f) Correlation of VAR index with BP

Fig. 11. Scatter plot between TIs and properties of the drugs

where $\alpha_6 = 574341021.4219$, $\alpha_5 = 1980185583.7934$, $\alpha_4 = 2822657956.7383$,

$\alpha_3 = 2129137129.2698, \alpha_2 = 896257438.2624, \alpha_1 = 199616275.3451$and $\beta_2 = 18377312$.

The equation obtained between MR vs VAR is as follows;

$$MR = \alpha_6(VAR)^6 - \alpha_5(VAR)^5 + \alpha_4(VAR)^4 - \alpha_3(VAR)^3 + \alpha_2(VAR)^2 - \alpha_1(VAR) + \beta_3, \tag{4}$$

where $\alpha_6 = 527474636.7127$, $\alpha_5 = 1749587979.9320$, $\alpha_4 = 2404445723.5146$,

$\alpha_3 = 1752208246.5926, \alpha_2 = 714036239.2036, \alpha_1 = 13803019.5391$and $\beta_3 = 13803019$.

The equation obtained between PSA vs VAR is as follows;

$$PSA = \alpha_6(VAR)^6 - \alpha_5(VAR)^5 + \alpha_4(VAR)^4 - \alpha_3(VAR)^3 + \alpha_2(VAR)^2 - \alpha_1(VAR) + \beta_4, \tag{5}$$

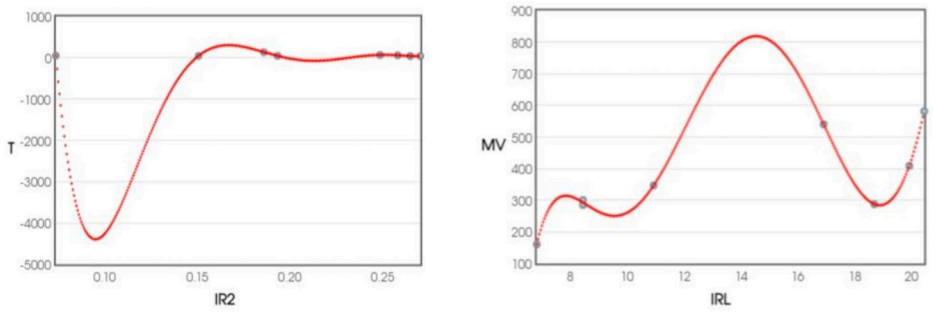

(a) Correlation of IR2 index with T (b) Correlation of IRL index with MV

Fig. 12. Scatter plot of TIs against T and MV

where $\alpha_6 = 660863774.0586$, $\alpha_5 = 2198956762.4778$, $\alpha_4 = 3035709313.8916$,

$\alpha_3 = 2225200580.4419, \alpha_2 = 913231000.8994, \alpha_1 = 198923151.7951$and $\beta_4 = 17963825$.

The equation obtained between P vs VAR is as follows;

$$P = \alpha_6(VAR)^6 - \alpha_5(VAR)^5 + \alpha_4(VAR)^4 - \alpha_3(VAR)^3 + \alpha_2(VAR)^2 - \alpha_1(VAR) + \beta_5, \tag{6}$$

where $\alpha_6 = 209772391.8457$, $\alpha_5 = 695786123.7815$, $\alpha_4 = 956197186.7151$,

$\alpha_3 = 696803056.2546$, $\alpha_2 = 283946061.7945$, $\alpha_1 = 61342938.0875$and $\beta_5 = 5488718$.

The equations obtained between T vs VAR and T vs IR_2 are as follows;

$$T = \alpha_5(VAR)^5 + \alpha_4(VAR)^4 - \alpha_3(VAR)^3 + \alpha_2(VAR)^2 - \alpha_1(VAR) + \beta_6, \tag{7}$$

where $\alpha_5 = -11134749.8385$, $\alpha_4 = 32176507.3426$, $\alpha_3 = 36871157.3849$,

$\alpha_2 = 20936252.9427$, $\alpha_1 = 5889594.1456$ and $\beta_6 = 656685.9456$.

$$T = \alpha_6(IR_2)^6 - \alpha_5(IR_2)^5 + \alpha_4(IR_2)^4 - \alpha_3(IR_2)^3 + \alpha_2(IR_2)^2 - \alpha_1(IR_2) + \beta_7, \tag{8}$$

where $\alpha_6 = 8688348552.6058$, $\alpha_5 = 10369413759.3853$, $\alpha_4 = 5029282934.2713$,

$\alpha_3 = 1262426363.5738, \alpha_2 = 171750161.0431, \alpha_1 = 11880534.9052$ and $\beta_7 = 320798.4392$.

The equations obtained between MV vs $IRDIF$, MV vs IRL and MV vs IRD_1 are as follows;

$$MV = \alpha_5(IRDIF)^5 - \alpha_4(IRDIF)^4 + \alpha_3(IRDIF)^3 - \alpha_2(IRDIF)^2 - \alpha_1(IRDIF) + \beta_8, \tag{9}$$

where $\alpha_5 = 0.0015$, $\alpha_4 = 0.0758, \alpha_3 = 1.4023$, $\alpha_2 = 1.0339, \alpha_1 = 183.4683$and $\beta_8 = 1190.2864$.

$$MV = \alpha_6(IRL)^6 + \alpha_5(IRL)^5 - \alpha_4(IRL)^4 + \alpha_3(IRL)^3 - \alpha_2(IRL)^2 + \alpha_1(IRL) - \beta_9, \tag{10}$$

where $\alpha_6 = -0.0138$, $\alpha_5 = 1.2445$, $\alpha_4 = 44.8583$, $\alpha_3 = 825.8360$,

$\alpha_2 = 8182.2296$, $\alpha_1 = 41427.8308$ and $\beta_9 = 83698.607$.

$$MV = \alpha_6(IRD_1)^6 - \alpha_5(IRD_1)^5 + \alpha_4(IRD_1)^4 - \alpha_3(IRD_1)^3 + \alpha_2(IRD_1)^2 - \alpha_1(IRD_1) + \beta_{10}, \tag{11}$$

where $\alpha_6 = 0.0022$, $\alpha_5 = 0.2363$, $\alpha_4 = 10.1241$, $\alpha_3 = 223.4032$,

$\alpha_2 = 2671.4539$, $\alpha_1 = 16364.8873$ and $\beta_{10} = 40248.3902$.

It was discovered that IR_2 has a good association with the estimated 50% inhibitory concentration IC50 values after the polynomial regression models were briefly applied to the inhibitor and suggested index.

$$IC50 = -41656738.22(IR_2)^5 + 39351097(IR_2)^4 - 14319440.56(IR_2)^3 + 2487953.03(IR_2)^2 - 203919.65(IR_2) + 6182.86. \tag{12}$$

The polynomial model (12) of the $IR2$ index and the 50% inhibitory concentration IC50 values is presented in Fig. 13. For the studied medicines, Table 7 displays the observed IC50 from model (12) together with the anticipated activity estimated using the curve fitting model.

Table 6
The adj R^2 values for the fitted curve of topological descriptors against the properties of COVID-19 drugs.

Topological descriptors	BP	E	FP	MR	PSA	P	T	MV
VAR	0.9761	0.979	0.976	0.9973	0.9105	0.9974	0.9991	0.994
AL	-	-	0.6499	0.6486	-	0.649	-	0.874
IR_1	-	0.6177	0.9538	0.8571	-	0.857	-	0.9956
IR_2	-	-	0.6264	0.8676	0.6283	0.8663	0.999	0.8668
IRF	-	-	0.9488	-	-	-	-	0.8009
IRFW	-	0.6376	0.93	0.6678	-	0.6672	-	0.9388
IRA	-	-	-	-	-	-	0.9875	-
IRB	-	-	-	-	-	-	-	0.8498
IRC	0.681	0.6591	-	-	-	0.9788	0.726	-
IRDIF	-	-	0.9561	0.8761	-	0.8765	-	0.9969
IRL	-	-	0.9561	0.8342	-	0.8347	-	0.9969
IRLU	-	-	-	0.6716	-	0.6712	-	0.7458
IRLF	-	-	0.9561	0.8554	-	0.8558	-	0.9955
IRLA	0.63	0.6655	0.969	0.8145	-	0.815	-	0.9965
IRD_1	-	-	0.9561	0.8151	-	0.8156	-	0.9969
IRGA	-	-	-	-	-	-	-	-

Table 7
Drugs for COVID with predicted and experimental IC50 values.

Drugs	IC50(μ M)	Predicted IC50 using model (12)	Residual
Lopinavir	5.25	-138252764491.65	138252764496.9
Ritonavir	8.63	-1784811742621.96	1784811742630.59
Arbidol	3.53	-17322156839.6858	17322156843.2158
Chloroquine	1.38	-98941339.29	98941340.67
Hydroxy-Chloroquine	0.72	-1680665.58	1680666.3
Theaflavin	8.44	-1592768014194.76	1592768014203.2
Remdesivir	0.98	-12639764.28	12639765.27

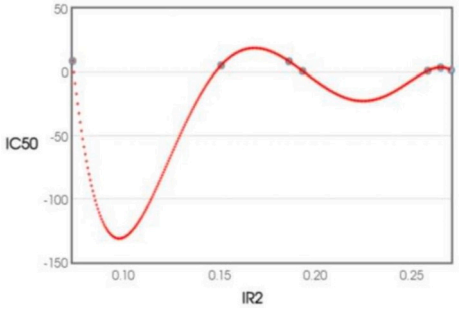

Fig. 13. Scatter plot between IR_2 and IC50.

5. Conclusion

Start by understanding the theoretical underpinnings of the topological index you're studying. Each index is based on specific mathematical relationships that reflect certain structural or connectivity aspects of molecules. Relate the index to the underlying chemical and physical properties it is expected to capture. For example, consider how the index might relate to molecular size, shape, branching, connectivity, or electronic properties. Our investigation of the suggested indices in Section 1 has shown us that Table 6 and Figures (Fig. 11 and Fig. 12) that

• The properties B_P, E, F_P, M_R, PS_A and P can be predicted using only VAR index as the corresponding adj. R^2 values are 0.9761, 0.979, 0.976, 0.9973, 0.9105, and 0.9974, respectively. As a result, the VAR index is ideal for forecasting these six physical qualities.
• The property T can be predicted using VAR, IR_2 and IRA indices as the corresponding adj. R^2 values are 0.9991, 0.999, and 0.9875, respectively. We can see that both VAR and IR_2 are the best-suited predictors for T.
• For the property MV can be predicted using VAR, $IR_1, IRFW, IRDIF, IRL, IRLF, IRLA$ and IRD_1 indices as the corresponding adj. R^2 values are 0.994, 0.9956, 0.9388, 0.9969, 0.9969, 0.9955, 0.9965, and 0.9965, respectively. We can observe that the $IRDIF$ IRL and IRD_1 are the best-suited predictors for MV. The physical interpretation of topological indices can provide insights into various properties and behaviors of molecules, networks, or structures.

Funding Statement

This research is supported by United Arab Emirates University (UAEU), Al Ain, UAE via Grant No. G00003739.

CRediT authorship contribution statement

Muhammad Usman Ghani: Writing – original draft. **Muhammad Imran:** Funding acquisition, Project administration, Validation, Writing – review & editing. **S. Sampathkumar:** Conceptualization, Validation. **Fairouz Tchier:** Data curation, Visualization. **K. Pattabiraman:** Data curation, Software. **Ahmad Zubair Jan:** Formal analysis, Investigation.

Declaration of competing interest

The authors declare that there is no conflict of interest regarding the publication of this article. All the authors of the paper have agreed to submit this paper. With best regards

Data availability

No data was used for the research described in the article.

Acknowledgement

Researchers Supporting Project number (RSP2023R401), King Saud University, Riyadh, Saudi Arabia.

References

[1] Sumaira Manzoor, et al., Flowery ln2MnSe4 novel electrocatalyst developed via anion exchange strategy for efficient water splitting, Nanomaterials 12 (13) (2022) 2209.
[2] Nadeem Abbas, et al., Mathematical model of temperature-dependent flow of power-law nanofluid over a variable stretching Riga sheet, in: Waves in Random and Complex, Media, 2022, pp. 1–18.
[3] Muhammad Hassan, et al., Structural parameters, energy states and magnetic properties of the novel Se-doped NiFe2O4 ferrites as highly efficient electrocatalysts for HER, Ceram. Int. 48 (17) (2022) 24866–24876.
[4] Taqi A.M. Shatnawi, Nadeem Abbas, Wasfi Shatanawi, Comparative study of Casson hybrid nanofluid models with induced magnetic radiative flow over a vertical permeable exponentially stretching sheet, AIMS Math. 7 (12) (2022) 20545–20564.
[5] Munirah Abdullah Almessiere, et al., Manganese/yttrium codoped strontium nanohexaferrites: evaluation of magnetic susceptibility and mossbauer spectra, Nanomaterials 9 (1) (2018) 24.
[6] Aqsa Nazir, Nadeem Abbas, W. Shatanawi, On stability analysis of a mathematical model of a society confronting with internal extremism, Int. J. Mod. Phys. B 37 (07) (2023) 2350065.
[7] M.V. Zdorovets, et al., Phase transformations in FeCo–Fe2CoO4/Co3O4-spinel nanostructures as a result of thermal annealing and their practical application, J. Mater. Sci., Mater. Electron. 32 (12) (2021) 16694–16705.
[8] Taqi A.M. Shatnawi, Nadeem Abbas, Wasfi Shatanawi, Mathematical analysis of unsteady stagnation point flow of radiative Casson hybrid nanofluid flow over a vertical Riga sheet, Mathematics 10 (19) (2022) 3573.
[9] K.K. Kadyrzhanov, et al., Research of the shielding effect and radiation resistance of composite CuBi 2 O 4 films as well as their practical applications, J. Mater. Sci., Mater. Electron. 31 (2020) 11729–11740.
[10] Nadeem Abbas, et al., Theoretical analysis of induced MHD Sutterby fluid flow with variable thermal conductivity and thermal slip over a stretching cylinder, AIMS Math. 8 (5) (2023) 10146–10159.
[11] Reda E. El-Shater, et al., Fabrication of doped ferrites and exploration of their structure and magnetic behavior, Mater. Adv. (2023).
[12] Nadeem Abbas, et al., Numerical analysis of Darcy resistant Sutterby nanofluid flow with effect of radiation and chemical reaction over stretching cylinder: induced magnetic field, AIMS Math. 8 (2023) 11202–11220.
[13] A.L. Kozlovskiy, M.V. Zdorovets, Synthesis, structural, strength and corrosion properties of thin films of the type CuX (X= Bi, Mg, Ni), J. Mater. Sci., Mater. Electron. 30 (2019) 11819–11832.
[14] Anna Kotelnikova, et al., The influence of saccharin adsorption on NiFe alloy film growth mechanisms during electrodeposition, RSC Adv. 12 (55) (2022) 35722–35729.
[15] A.L. Kozlovskiy, M.V. Zdorovets, Effect of doping of Ce4+/3+ on optical, strength and shielding properties of (0.5-x) TeO2-0.25 MoO-0.25 Bi2O3-xCeO2 glasses, Mater. Chem. Phys. 263 (2021) 124444.
[16] Ahmed Maher Henaish, et al., Structure and optoelectronic properties of ferroelectric PVA-PZT nanocomposites, Opt. Mater. 138 (2023) 113402.
[17] Olena S. Yakovenko, et al., Magnetic anisotropy of the graphite nanoplatelet–epoxy and MWCNT–epoxy composites with aligned barium ferrite filler, J. Mater. Sci. 52 (2017) 5345–5358.
[18] O.S. Yakovenko, et al., Electrophysical properties of epoxy-based composites with graphite nanoplatelets and magnetically aligned magnetite, Mol. Cryst. Liq. Cryst. 661 (1) (2018) 68–80.
[19] Ying-Fang Zhang, et al., Connecting SiO 4 in silicate and silicate chain networks to compute kulli temperature indices, Molecules 27 (21) (2022) 7533.
[20] S.V. Trukhanov, D.P. Kozlenko, A.V. Trukhanov, High hydrostatic pressure effect on magnetic state of anion-deficient La0. 70Sr0. 30MnOx perovskite manganites, J. Magn. Magn. Mater. 320 (14) (2008) e88–e91.
[21] Muhammad Usman Ghani, et al., A paradigmatic approach to find the valency-based K-banhatti and redefined Zagreb entropy for niobium oxide and a metal–organic framework, Molecules 27 (20) (2022), nanocomposites doped with Nb2O5." Sensors 20(17) (2020) 4851.
[22] A. Kozlovskiy, K. Egizbek, M.V. Zdorovets, M. Ibragimova, A. Shumskaya, A.A. Rogachev, Z.V. Ignatovich, K. Kadyrzhanov, Evaluation of the efficiency of detection and capture of manganese in aqueous solutions of FeCeOx nanocomposites doped with Nb2O5, Sensors 20 (2020) 4851.
[23] S.V. Trukhanov, et al., Cation ordering and magnetic properties of neodymium-barium manganites, Tech. Phys. 53 (2008) 49–54.
[24] A. Kozlovskiy, et al., Optical and structural properties of AlN ceramics irradiated with heavy ions, Opt. Mater. 91 (2019) 130–137.
[25] Özge Çolakoglu Havare, Topological indices and QSPR modeling of some novel drugs used in the cancer treatment, Int. J. Quant. Chem. 121 (2021) 24, e26813.

[26] Sina Abbasi, Çigdem Sicakyüz, Babek Erdebilli, Designing the home healthcare supply chain during a health crisis, J. Eng. Res. (2023) 100098.
[27] Sourav Mondal, Nilanjan De, Anita Pal, Topological indices of some chemical structures applied for the treatment of COVID-19 patients, Polycycl. Aromat. Compd. 42 (4) (2022) 1220–1234.
[28] Sina Abbasi, Maryam Daneshmand-Mehr, Armin Ghane Kanafi, Green closed-loop supply chain network design during the coronavirus (COVID-19) pandemic: a case study in the Iranian automotive industry, Environ. Model. Assess. 28 (1) (2023) 69–103.
[29] Seyed Mahmoud Sheikholeslami, Akbar Jahanbani, Zehui Shao, On the molecular structure of Remdesivir for the treatment of Covid-19, Comput. Methods Biomech. Biomed. Eng. 24 (9) (2021) 995–1002.
[30] Muhammad Usman Ghani, et al., Hex-derived molecular descriptors via generalised valency-based entropies, IEEE Access (2023).
[31] Abdul Rauf Khan, et al., Fundamental aspects of skin cancer drugs via degree-based chemical bonding topological descriptors, Molecules 28 (9) (2023) 3684.
[32] Sina Abbasi, Hassan Ahmadi Choukolaei, A systematic review of green supply chain network design literature focusing on carbon policy, Decis. Anal. J. (2023) 100189.
[33] Sina Abbasi, et al., Performance measurement of the sustainable supply chain during the COVID-19 pandemic: a real-life case study, Found. Comput. Decision Sci. 47 (4) (2022) 327–358.
[34] Xie Chang, et al., Molecular irregularity indices of nanostar, fullerene, and polymer dendrimers, J. Chem. 2020 (2020) 1–12.
[35] Micheal Arockiaraj, et al., Entropy structural characterization of zeolites BCT and DFT with bond-wise scaled comparison, Sci. Rep. 13 (1) (2023) 10874.
[36] Sina Abbasi, Environmental impact assessment with rapid impact assessment matrix method during the COVID-19 pandemic: a case study in Tehran, 2023.
[37] Sina Abbasi, Maryam Daneshmand-Mehr, K. Ghane, Designing a tri-objective, sustainable, closed-loop, and multi-echelon supply chain during the COVID-19 and lockdowns, Found. Comput. Decision Sci. 48 (2023) 1.
[38] Muhammad Usman Ghani, et al., Characterizations of chemical networks entropies by K-banhatii topological indices, Symmetry 15 (1) (2023) 143.
[39] Muhammad Usman Ghani, et al., Entropies via various molecular descriptors of layer structure of H 3 BO 3, Mathematics 10 (24) (2022) 4831.
[40] M.A. Basit, et al., Numerical simulation of bioconvective Casson nanofluid through an exponentially permeable stretching surface, Int. J. Mod. Phys. B (2023) 2450128.
[41] Muhammad Abdul Basit, et al., Partial differential equations modeling of bio-convective sutterby nanofluid flow through paraboloid surface, Sci. Rep. 13 (1) (2023) 6152.
[42] Umar Farooq, et al., Recent progress in Cattaneo-Christov heat and mass fluxes for bioconvectional Carreau nanofluid with motile microorganisms and activation energy passing through a nonlinear stretching cylinder, Ain Shams Eng. J. (2023) 102316.
[43] S. Prabhu, et al., Computational analysis of some more rectangular tessellations of kekulenes and their molecular characterizations, Molecules 28 (18) (2023) 6625.
[44] Rashad Ismail, et al., A novel perspective for M-polynomials to compute molecular descriptors of borophene nanosheet, Sci. Rep. 13 (1) (2023) 12016.